Soil Reinforcement under Oblique Pull - An Updated Discretization

S. Patra[1] and J.T. Shahu[2]
[1] *School of Engineering, Indian Institute of Technology Mandi, Mandi, India*
[2] *Department of Civil Engineering, Indian Institute of Technology Delhi, New Delhi, India*
E-mail: shahu@civil.iitd.ac.in

ABSTRACT: Reinforced soil structures are gaining popularity for a variety of reasons mainly because it is safe, economical, aesthetic and rapid in constructions. However, the actual behaviour of these structures at failure is still not properly understood. The present study attempts to evaluate the internal stability of these structures against pullout failure. Kinematics of failure suggests that the failure surface intersects the reinforcement obliquely causing an oblique pullout of the reinforcement. In this paper, an updated discretization technique is used to determine the pullout capacity of an inextensible reinforcement resting on a linear elastic Pasternak subgrade and subjected to an oblique end force. A parametric study is conducted and a new factor, length correction factor is introduced in the present analysis. The correction factors have a significant influence on the pullout response especially for high values of obliquity and end displacement. Present analysis thus gives a more realistic value of pullout capacity which is required for the internal stability analysis and design of reinforced soil structures. A case study is also presented to validate the proposed analysis. The maximum reinforcement tension is predicted for top few reinforcements using the proposed method and the AASHTO Simplified Method. The present analysis gives a better prediction of the mobilized reinforcement tension compared to the AASHTO method.

KEYWORDS: Numerical analysis, Discretization, Pullout capacity, Pasternak subgrade, Inextensible reinforcement, Rigid plastic interface.

1. INTRODUCTION

Reinforced soil structures such as reinforced soil walls and embankments (Figs. 1a and b) are gaining popularity as sustainable alternatives to the conventional concrete retaining structures since they are economical, easy and rapid to construct (Damians et al. 2016, Won et al. 2016). Stability and economy, however, are two major concerns considering their widespread use in critical infrastructure projects e.g. construction of highways and railways.

Internal stability of reinforced soil structures depends on the kinematics of failure where the failure surface intersects the reinforcement obliquely causing an oblique pullout of the reinforcement (Figure 1(a)-(c)) (Gao et al. 2014; Sitar et al. 2005; Madhav and Umashankar 2003; MacLaughlin et al. 2001). But, conventional methods of analyses consider only the axial direction of the pullout force (i.e., □ = 0 and □ = 0, refer Figure 1c) and do not account for the obliquity of the pullout force and resulting complex soil-reinforcement interaction. Consequently, these methods fail to predict the soil-wall response accurately and yield a highly conservative value of the factor of safety at pullout (Rowe and Ho 1993; Madhav and Umashankar 2003; Patra and Shahu 2012; Bathurst et al. 2009; Allen and Bathurst 2013; Ouria et al. 2016; Yu et al. 2016).

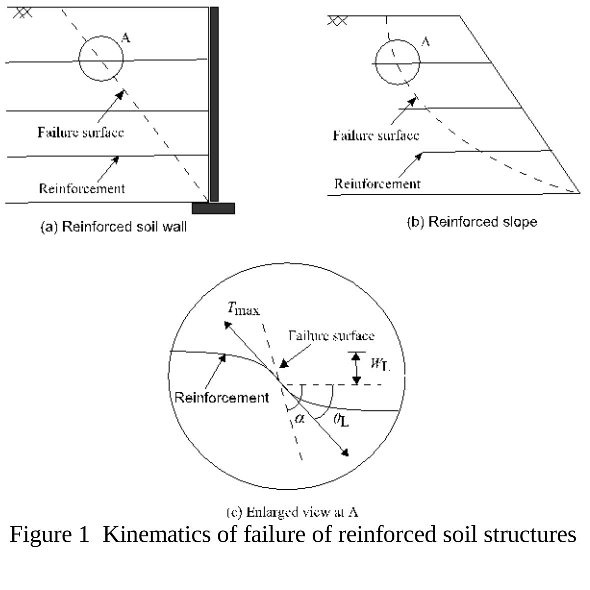

Figure 1 Kinematics of failure of reinforced soil structures

The effect of obliquity of the pullout force on the internal stability of reinforced soil wall was first reported by Madhav and Umashankar (2003). The analysis considered the response of an inextensible reinforcement resting on a set of Winkler's springs and subjected to the transverse component of the oblique pullout force. The horizontal component of the pullout force was neglected altogether. The equilibrium of forces was applied assuming the soil-reinforcement interface acting along the horizontal projection of the deformed reinforcement and not along the final deformed shape of the reinforcement. Consequently, the analysis was valid for small end-displacement only.

Shahu (2007) removed the above anomaly and presented a Winkler's based model for the pullout analysis of inextensible reinforcement subjected to an oblique end-force. The equilibrium of forces was applied considering the interface stresses acting along the deformed shape of the reinforcement. However, the model suffers from the inherent drawbacks of Winkler spring based model which assumes that displacements occur only under the loaded area. Patra and Shahu (2012) removed the above shortcomings by presenting a Pasternak subgrade based model for the oblique pullout analysis.

In all of the above instances, the displacement compatibility is disregarded. For inextensible reinforcement, the fundamental premise is that the length of the reinforcement remains unchanged throughout the pullout. To satisfy the compatibility condition, there must be a rigid body movement of the far-end point A (Figure 2a) of the reinforcement along the horizontal direction in response to the transverse end-displacement w_L. The previous analyses however neglected this rigid body movement of point A associated with the transverse end-displacement. Therefore, the apparent deformed length is greater than the actual length of the reinforcement (i.e. initial length L for inextensible reinforcement). The larger apparent length contributes to a greater mobilization of normal and shear stresses which result in inaccurate prediction of the pullout capacity and end-displacement especially for higher values of the obliquity □ of the pullout force.

In this paper, a rational approach is presented for the analysis of inextensible sheet reinforcement subjected to an oblique end-force. The reinforcement is assumed to be a rough membrane resting on a linear elastic Pasternak subgrade. An updated discretization technique is proposed to determine the exact deformed shape of the reinforcement and its influence on the pullout responses, namely, pullout capacity, end-displacement, and end-inclination. The analysis considers a proper soil-reinforcement interaction by assuming a rigid-plastic interface response. A new factor, length correction factor, is introduced in the present analysis. The effect of the length correction factor on the pullout behaviour is also studied in detail. A case study is also presented to validate the proposed analysis. The maximum reinforcement tension is predicted for top few reinforcements, which are critical in a pullout, using the proposed method and the AASHTO Simplified Method.

2. OBLIQUE PULLOUT ANALYSIS

2.1 Problem Definition

Figure 2(a) shows an inextensible reinforcement of length L embedded at depth D. The reinforcement is assumed to be a rough membrane resting on a linear elastic Pasternak subgrade. The Pasternak subgrade represents a shear layer resting on a set of Winkler's springs (Figure 2b) and mathematically expressed as follows (Vlazov 1966; Selvadurai 1979):

$$p - q = k_s w - GH\frac{d^2w}{dx^2} \tag{1}$$

where q and p are normal stresses at the top and bottom of the reinforcement, k_s = spring constant, and G = shear modulus.

The reinforcement is subjected to an oblique pullout force P making an obliquity α at a point B where the sliding mass intersects the reinforcement. Under the action of the oblique pullout force P, the reinforced mobilized maximum tension $T_{\max}$ at pullout end B in the direction θ_L with the horizontal (Figure 2(b)). The deformed shape of the reinforcement is shown in Figure 2(c) where the normal and shear stresses at the top of the reinforcement are p and f_1 and at the bottom q and f_2.

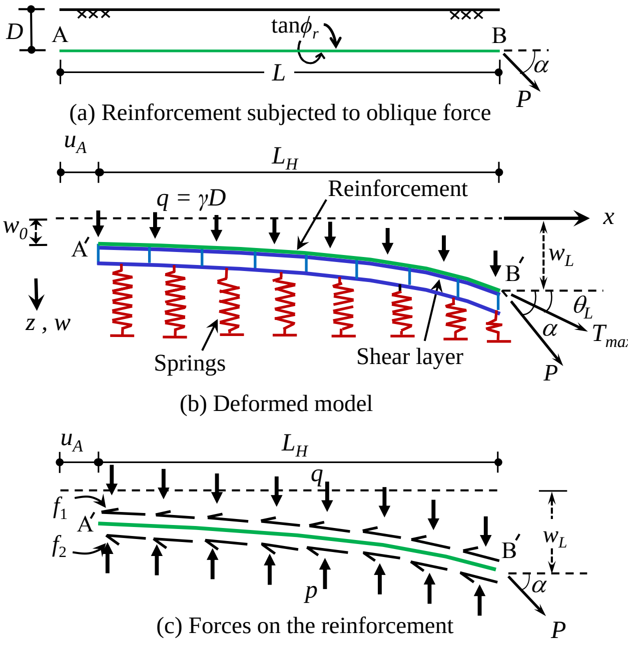

Figure 2 Mechanistic model (Patra and Shahu 2012)

2.1.1 Updated discretization scheme

An updated discretization technique is adopted in the analysis to account for the exact deformed shape of the reinforcement. In the earlier analysis (Madhav and Umashankar 2003; Shahu 2007; and Patra and Shahu 2012), the discretized length was assumed to be a constant horizontal distance equal to the initial length L of the reinforcement (Figure 3). However, an inextensible reinforcement, under the influence of any transverse end-displacement, undergoes a rigid body displacement in the horizontal direction so that the deformed length of the reinforcement remains constant. However, the horizontal projected length L_H (Figure 3) of the deformed reinforcement reduces due to this rigid body displacement u_A and is less than the initial length L of the reinforcement. Therefore, the discretization should be done over this changed projected length L_H as shown in Figure 3. In the present analysis, the above modification is incorporated using an updated discretization scheme where the discretization is redone in each iteration with respect to the changed projected length (A-A') and the boundary conditions are modified accordingly (Figure 3), i.e. the boundary condition is now applied to the point A' instead of A (refer section 2.3).

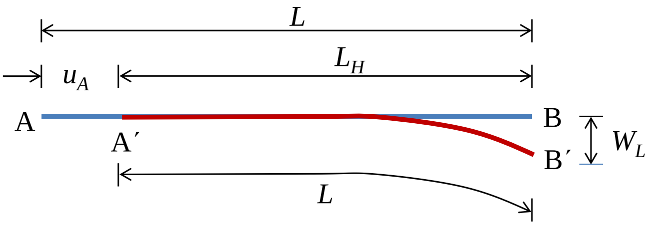

Figure 3 Deformed and projected length of reinforcement

2.2 Formulations

Figure 4(a) shows a reinforcement element of infinitesimal horizontal length dx and unit width. The reinforcement tensions and inclinations at horizontal distances x and (x+Δx) are T and θ, and (T+ΔT) and (θ+$\Delta\theta$), respectively. The normal and shear stresses at the top of the reinforcement are p and f_1 and at the bottom q and f_2.

Applying vertical and horizontal force equilibrium to the final deformed shape of the reinforcement element and using the equation for Pasternak subgrade (Eq. 1, Figure 4(b)), one gets following basic governing equation as given by Patra and Shahu (2012)

$$\frac{dT}{dx} = \left(k_s w - GH\frac{d^2w}{dx^2} + 2\gamma D\right)\tan\phi_r + \left(k_s w - GH\frac{d^2w}{dx^2}\right)\tan\theta \tag{2}$$

$$T\cos^2\theta\left(\frac{d^2w}{dx^2}\right) = k_s w - GH\frac{d^2w}{dx^2} \tag{3}$$

The boundary conditions for this problem are (Figure 2(b)): at $x = 0$ (end A), $dw/dx = 0$ and $T = 0$; and at $x = L$ (end B), $w = w_L$.

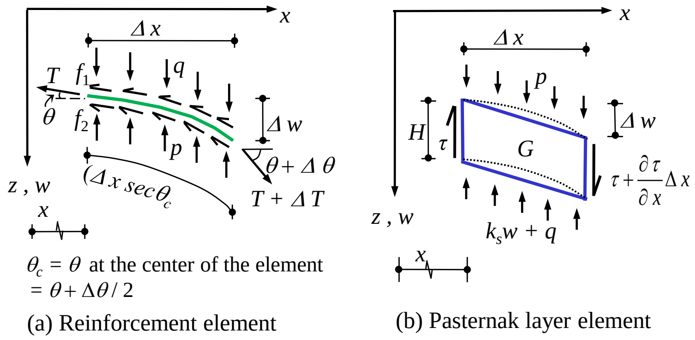

Figure 4 Soil-reinforcement elements (Patra and Shahu 2012)

Nondimensionalizing and discretizing Wang (Anderson 1982) the above governing differential equations and finally simplifying (Patra and Shahu 2012), one gets the following expressions for reinforcement tension and displacement at each node

$$T^*_{i+1} = T^*_i + \frac{0.5}{n}\left[\left\{\mu W_i W_L - n^2 G^* W_L \left(W_{i+1} - 2W_i + W_{i-1}\right)\right\}\left(\frac{\tan\theta_i}{\tan\phi_r} + 1\right) + 2\right] \tag{4}$$

$$W_i = \frac{n^2\left(W_{i+1}+W_{i-1}\right)\left(2T_i^* \tan\phi_r \cos^2\theta_i + G^*\right)}{\mu + 2n^2\left(2T_i^* \tan\phi_r \cos^2\theta_i + G^*\right)} \quad (5)$$

where μ = subgrade normal stiffness factor; G^* = subgrade shear stiffness factor; $W_L = w_L/L$ = normalized end displacement, $T^* = T/T_{HP}$ where $T_{HP} = 2\gamma DL\tan\phi_r$ is the axial pullout capacity of the reinforcement, $X = x/L$ and i is the number of elements into which the reinforcement sheet is divided.

The assumed boundary conditions are (refer Shahu 2007; Patra and Shahu 2012):

at $X = 0$, $dw/dx=0$ and $T^*= 0$; and at $X =1.0$, $W = 1.0$ (6)

Considering the overall equilibrium of forces on the deformed reinforcement (Figure 2c) and after nondimensionalizion, discretization and simplifying, one gets (Patra and Shahu 2012)

$$\tan\alpha = \frac{\left[\frac{1}{\tan\phi_r}\sum_{i=1}^{n}\frac{\mu W_i W_L}{\cos\theta_{ci}} + \sum_{i=1}^{n}\left\{\mu W_i W_L + 2 - n^2 G^* W_L\left(W_{i+1} - 2W_i + W_{i-1}\right)\right\}\sin\theta_{ci}\right]}{\sum_{i=1}^{n}\left[\left\{\mu W_i W_L + 2 - n^2 G^* W_L\left(W_{i+1} - 2W_i + W_{i-1}\right)\right\}\cos\theta_{ci}\right]} \quad (7)$$

$$P^* = \frac{1}{2n\cos\alpha}\sum_{i=1}^{n}\left[\left\{\mu W_i W_L + 2 - n^2 G^* W_L\left(W_{i+1} - 2W_i + W_{i-1}\right)\right\}\cos\theta_{ci}\right] \quad (8)$$

where $P^* = P/T_{HP}$, $\theta_{ci} = \tan^{-1}\left[nW_L\left(W_{i+1} - W_i\right)/2\right]$ = value of θ_c for element i; and $\theta_i = \left(\theta_{ci} + \theta_{ci-1}\right)/2$

2.3 Solutions

The displacement W_i and tension T_i^* at any node i, are obtained by solving Eqs. (4) and (5) in conjunction with the boundary condition (Eq. 6) and overall equilibrium equations (Eqs. 7 and 8). A trial and error procedure is adopted for the solution. For each successive iteration, the discretization is redone with respect to the new projected length $L_{H,\,new}$ till it attain a constant value, where $L_{H,\,new}$ is given as

$$L_H, new = L\,L_H \Big/ \sum \frac{L_H^*}{N}\sec\theta_{ci} \quad (9)$$

Equation (9) is an empirical relation based on the deformation compatibility of the soil reinforcement response. The compatibility relation suggests that for an inextensible reinforcement, the length of the deformed reinforcement (= $\sum \frac{L_H^*}{N}\sec\theta_{ci}$) should be equal to the initial length L of the reinforcement irrespective of its transverse end displacement W_L (Figure 3). Thus, equation (9) gives a value of projected horizontal length $L_{H,new}$ iteratively when convergence is reached (i.e., $\sum \frac{L_H^*}{N}\sec\theta_{ci} = L$).

3. PARAMETRIC STUDY AND RANGE OF PARAMETERS

In the present analysis, a detailed parametric study is carried out to determine the influence of various model parameters on the pullout analysis. Sand having relative density: loose to dense is assumed as backfill material where detail geotechnical properties are shown in Table 1. Following ranges of geometric properties are also used in the analysis: reinforcement length L = 2-8 m, depth of reinforcement D = 1-10 m and subgrade layer thickness H_0 = 1-5 m (Patra and Shahu 2012). Considering the above equivalence of geotechnical (Table 1) and geometrical properties, Patra and Shahu (2012) suggest that the thickness of shear layer H = 0.09-0.54 m. The same is assumed in the present analysis. Patra and Shahu (2012) modified the shear layer thickness proposed by Vlazov and Leontiev (1966) (refer Patra and Shahu 2012; Selvadurai 1997) as $H = H_0/\lambda$. The factor λ was evaluated by comparing the load-settlement response and surface displacement profile of a rigid strip footing resting on an elastic half space as obtained from the finite-element (FE) analysis and the Pasternak model. The value of λ was found to vary from 11.17 to 9.24 (with an average value 10.02) for subgrade layer thickness H_0 ranging from 1- 5 m and resulting shear layer thickness was found to be H = 0.09-0.54 m (Table 1).

For the range of parameters used in Table 1 and the above geometric properties, the values of nondimensional subgrade modulus in vertical compression μ and shear G^* becomes 27 to 43,615 and 0.215 to 421, respectively. However, for the present analysis, the following range of controlling parameters is adopted: μ = 50-1000, G^* = 0-100, interface frictional angle ϕ_r = 20-45, based on the practical consideration as suggest by Patra and Shahu (2012).

Table 1 Ranges of Parameters (Patra and Shahu 2012)

Parameters	**Sand type**	
Relative density	Loose	Dense
E (MPa)	10	81
k_s (kN/m^3)	2692	109038
G (kPa)	3846	31154
H (m)	0.09 – 0.54	
ϕ_r (degrees)	20 – 45	
α (degrees)	0 – 85	

4. RESULTS AND DISCUSSION

4.1 Displacement and Tension Profile

Figures 5-6 display the displacement and tension profile of the reinforcement subjected to an oblique pullout force. The figures show the effect of length correction on the distribution of displacement and tension along the horizontal distance of the reinforcement.

Figure 5 demonstrate that under the transverse displacement, the far-off point A of the reinforcement (Figs. 2 and 3) experiences a rigid displacement u_A (distance between A to A', Figures. 2 and 3) along the horizontal direction. The magnitude of the rigid displacement u_A (Figures 2 and 3) is higher for a lower value of subgrade normal and shear stiffness factor but for a higher value of interface frictional resistance (Figure 5). The effect of length correction is mainly manifested with the rigid displacement of the reinforcement. For a particular combination of soil-reinforcement properties, a higher rigid displacement indicates a greater effect of length correction on the pullout response.

Higher the rigid displacement u_A, lower is the mobilized tension in the reinforcement (Figure 6). The decrease in reinforcement tension is more for lower values of G^* and μ, and higher values of α and ϕ_r. However, the tension in the reinforcement becomes more localized at the pullout end for higher values of the rigid displacement.

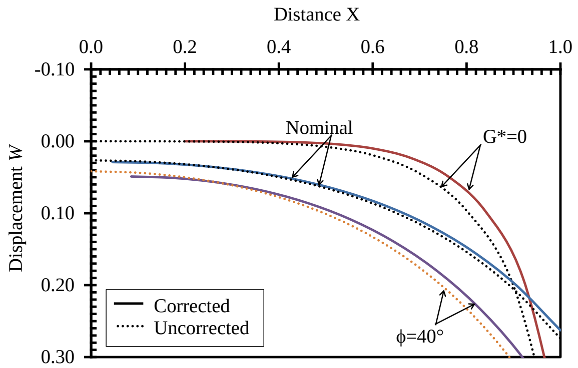

Figure 5 Displacement profile (Nominal case: G*=5, μ=50, ϕ=30°, α=60°, unless stated all other parameters remain unchanged as in the nominal case)

4.2 Localized Pullout Response

A detailed parametric study is carried out (Figures 7-17) to study the effect of various model parameters such as subgrade shear stiffness factor *G**, subgrade normal stiffness factor μ, interface frictional resistance ϕ_r and obliquity α on the pullout response. The effect of length correction on the pullout response is also quantified.

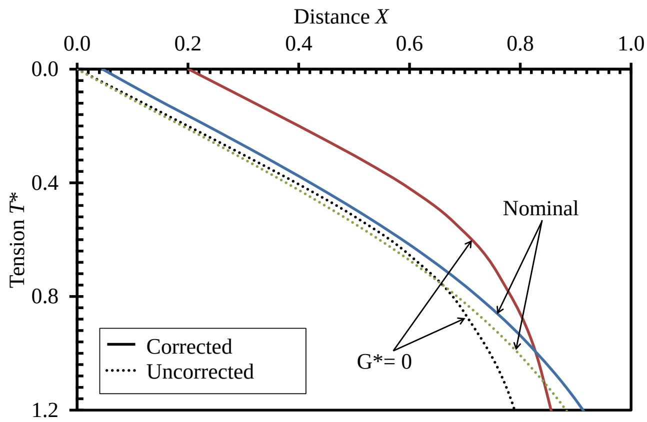

Figure 6 Reinforcement tension profile (Nominal case: G*=5, μ=50, ϕ=30°, α=60°, Unless stated all other parameters remain unchanged as in the nominal case)

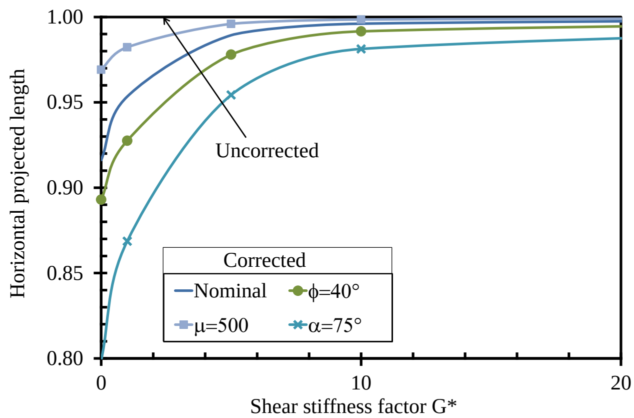

Figure 7 Effect of subgrade shear stiffness factor on horizontal projected length (Nominal case: μ=50, ϕ=30°, α=60°, Unless stated all other parameters remain unchanged as in the nominal case)

4.2.1 Effect of subgrade shear stiffness factor *G** – considering length correction

Figures 7-10 show the effect of subgrade shear stiffness factor *G**on the pullout response with and without considering the length correction. As *G** increases, the horizontal component of projected length increases (Figure 7) and becomes equal to 1.0 (i.e. the initial length of the reinforcement). For lower values of subgrade shear stiffness factor *G** and normal stiffness factor μ, but higher angle of interface friction ϕ_r; the effect is more

However, for lower subgrade shear stiffness factor *G** the horizontal projected length may become as low as eighty per cent of the initial length of the reinforcement.

Since at higher *G** the projected length of the reinforcement tends to reach the initial length of the reinforcement, all the responses namely, end displacement, mobilized maximum reinforcement tension and pullout capacity remain almost equal in both the cases: corrected and not corrected. However, the difference in the above responses increases for lower *G**. In other words, the effect of length correction is predominant for lower *G** (Figures 7-15).

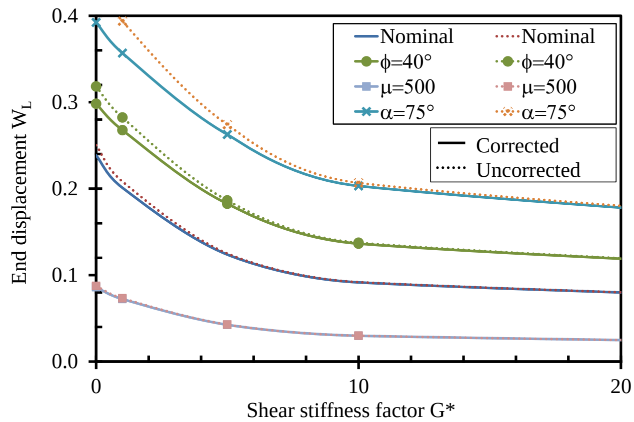

Figure 8 Effect of subgrade shear stiffness factor on end displacement W_L (Nominal case: μ=50, ϕ=30°, α=60°, Unless stated all other parameters remain unchanged as in the nominal case)

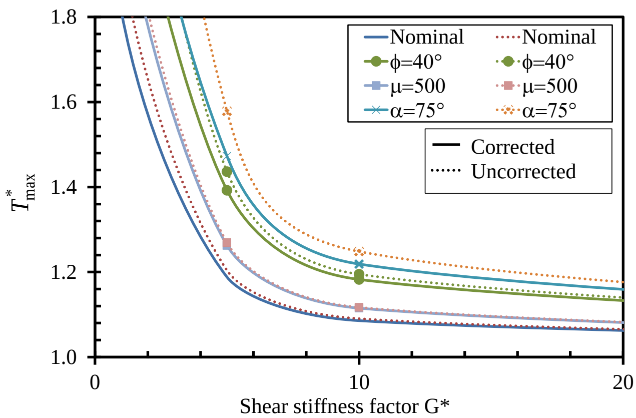

Figure 9 Effect of subgrade shear stiffness factor on maximum mobilized reinforcement tension T^*_{max} (Nominal case: μ=50, ϕ=30°, α=60°, Unless stated all other parameters remain unchanged as in the nominal case)

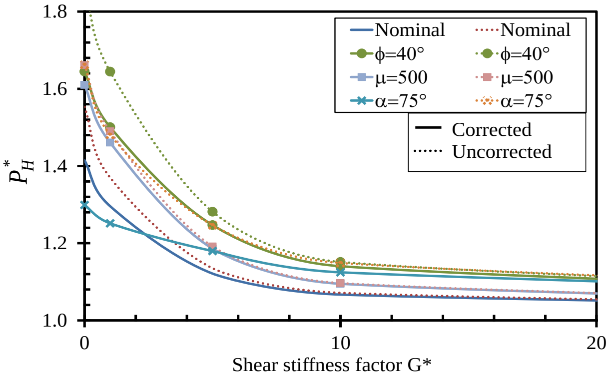

Figure 10 Effect of subgrade shear stiffness factor on horizontal component of pullout capacity P_H^* (Nominal case: μ=50, ϕ=30°, α=60°, Unless stated all other parameters remain unchanged as in the nominal case)

4.2.2 Effect of obliquity α – considering length correction

Figures 11-14 show the effect of obliquity on the pullout response with and without considering the length correction. Figure 11 shows that the as the obliquity α of the pullout force increases the projected length decreases. The effect is more for lower values of subgrade shear stiffness factor G^* and normal stiffness factor μ but higher angle of interface friction ϕ_r.

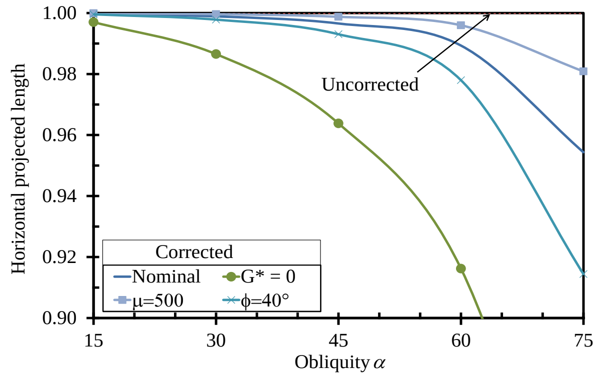

Figure 11 Effect of obliquity α on horizontal projected length (Nominal case: G*=5, μ=50, ϕ=30°, Unless stated all other parameters remain unchanged as in the nominal case)

Figures 12-14 show that all the corrected responses: end-displacement W_L, maximum mobilized reinforcement tension T^*_{max} and horizontal component of pullout capacity P_H^* are lower than the uncorrected values.

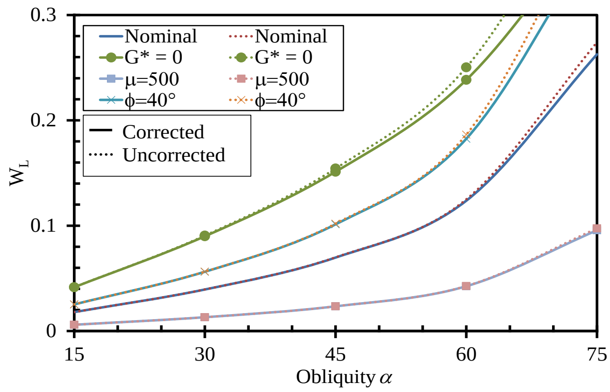

Figure 12 Effect of obliquity α on end-displacement W_L (Nominal case: G*=5, μ=50, ϕ=30°, Unless stated all other parameters remain unchanged as in the nominal case)

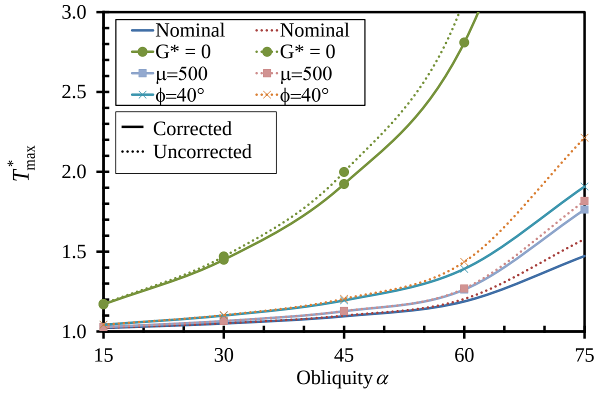

Figure 13 Effect of obliquity α on maximum mobilized reinforcement tension T^*_{max} (Nominal case: G*=5, μ=50, ϕ=30°)

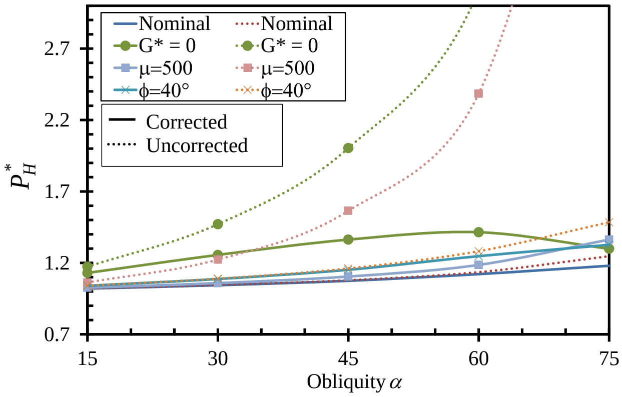

Figure 14 Effect of obliquity on horizontal component of oblique pullout force P_H^* (Nominal case: G*=5, μ=50, ϕ=30°, Unless stated all other parameters remain unchanged as in the nominal case)

Figure. 14 shows that as the obliquity α of the pullout capacity increases, the uncorrected values of horizontal component of the pullout capacity P_H^* goes on increasing. However, for a greater angle of obliquity α (> 60), the corrected pullout capacity again reduces which is also evident from the finite element analysis as shown by Shahu (2007). But, the earlier analyses by Shahu (2007); Patra and Shahu (2012) were unable to capture this behavior as they did not incorporate the length correction.

It can be explained as follows: as the angle of the obliquity α of the pulout force increases, the normal and shear stresses at the soil-reinforcement interface increase thereby the pullout capacity P_H^* increases. At the same time, with the increase in obliquity α there is an increase in the rigid body displacement u_A or, decrease in the projected length of the reinforcement. As the projected length reduces, there is a reduction in the mobilized reinforcement tension and horizontal component of oblique pullout capacity P_H^*. For a higher value of the obliquity α, the above reduction in the pullout capacity arisen from the lesser projected length may dominate over the increase in the pullout capacity due to the greater interface shear stresses.

4.3 Length correction factor LCF

A new factor, length correction factor (LCF) is defined in the present analysis. The effect of LCF on the pullout responses are shown in Figures 15-17. As the obliquity □ of the pullout force increases, the value of LCF reduces for all the responses: end displacement, maximum mobilized reinforcement tension and the horizontal pullout capacity. The effect of length correction is thus greater for higher values of obliquity and angle of interface friction and lower values of the normal and shear stiffness of the subgrade, thus demanding a greater reduction in the pullout responses.

For inextensible reinforcement and granular backfill, the pullout occurs at relatively lesser end displacement when subjected to an oblique pullout. Under such a small value of end displacement, the soil-reinforcement response usually shows a linear response. Thus, for inextensible reinforcement, the idealization of a conservative linear elastic model for subgrade does not results in significant error in the analysis as suggested by many researchers (Madhav and Umashankar 2003; Shahu 2007; Patra and Shahu 2012).

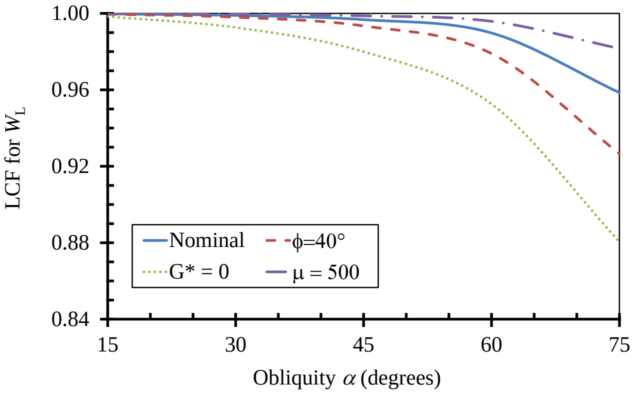

Figure 15 LCF for W_L and effect of obliquity (Nominal case: G*=5, μ=50, ϕ=30°, Unless stated all other parameters remain unchanged as in the nominal case)

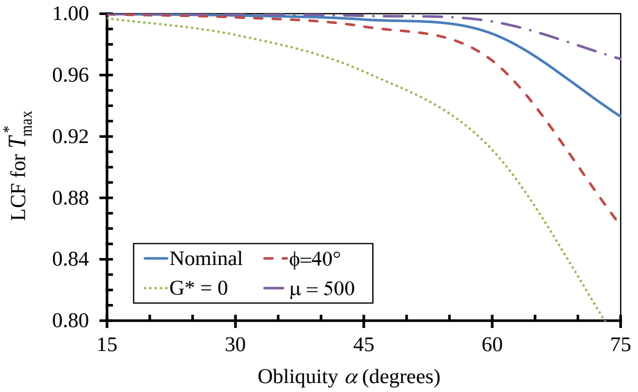

Figure 16 LCF for maximum mobilized reinforcement tension T^*_{max} and effect of obliquity (Nominal case: G*=5, μ=50, ϕ=30°, unless stated all other parameters remain unchanged as in the nominal case)

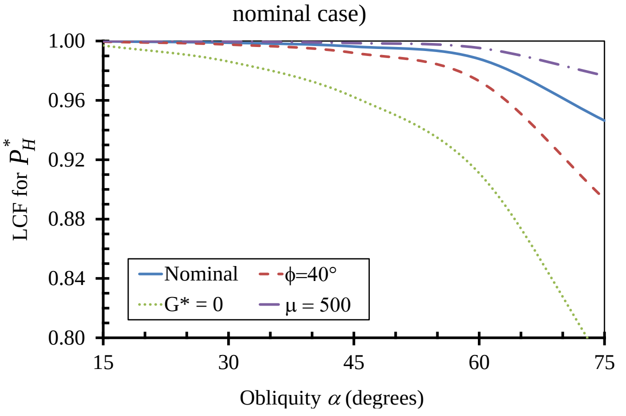

Figure 17 LCF for horizontal pullout capacity P^*_H and effect of obliquity (Nominal case: G*=5, μ=50, ϕ=30°, Unless stated all other parameters remain unchanged as in the nominal case)

5. CASE STUDY OF A REINFORCED SOIL WALL

A case study is presented for a 3.6 m height wall reinforced with welded wire mesh (WWM) (Bathurst et al. 2009). Bathurst et.al (2009) conducted model tests in a series of four full-scale modular block wall at RMC (Royal Military College of Canada) Retaining Wall Test Facility. The wall was reinforced with six layers of reinforcements using four different types of reinforcement: polypropylene (PP) geogrid (Model 1), modified polypropylene (Modified PP) geogrid (Model 2), less stiff polyester (PET) geogrid (Model 5) and stiff welded wire mesh (WWM) (Model 6) at a spacing of S_v = 0.6 m. The backfill was compacted using a vibrating plate tamper (light compaction) for model walls 5 and 6 and a heavier vibrating rammer (heavy compaction) for model walls 1 and 2. The modular block units of 300 mm long (toe to heel), 150 mm high and 200 mm wide were stacked at 8° batter from vertical. For the ease of construction and interpretation of test results, the walls were constructed on an instrumented rigid foundation having a stiff horizontal toe support. Bathurst et al. (2009) reported the horizontal and vertical displacement, horizontal toe load measurements and reinforcement tension in each layer at the end of construction and post-construction stage. Maximum surcharge levels varied from 85 to 130 kPa for the four walls during the post-construction stage. However, for comparing the measured and predicted loads, 50 kPa surcharge load and 30 mm post-construction serviceability limit proposed by Allen et al. (2003) for geosynthetic-reinforced soil walls with granular backfills was considered.

Model 6 reinforced with welded wire mesh is chosen for the present analysis as it exhibits an inextensible response. Backfill material was used as a uniformly graded, rounded beach sand with the bulk unit weight γ = 17.2 kN/m^3 and the peak friction angle ϕ =44° (Bathurst et al. 2005). The present analysis is used to predict the maximum mobilized reinforcement tension for top two layers of reinforcement as they are most critical in the pullout. The results are also compared with the AASHTO Simplified method (AASHTO 2002). The maximum reinforcement tension T_{max} is determined using the following expressions:

$$T_{max} = P^*_H K \gamma z S_V \tag{10}$$

Where P^*_H = horizontal pullout capacity factor (shown in Table 2) obtained from the solution of equations 4-9.

Figure 18 shows the present analysis predicts the maximum value of mobilized tension more accurately whereas AASHTO (2002) gives a conservative estimation of the same.

The interface frictional angle assumed in the present analysis is adopted from Bathurst et al. (2001). For predicting the same model test results (Model wall 6), Bathurst et al. (2001) assumed the interface frictional angle ϕ_r equal to the peak friction angle ϕ = 44°. The reinforcement used in the present analysis is welded wire mesh (Bathurst et al. 2001 and 2009). The load transfer mechanism for this type of reinforcement involves both frictional as well as passive resistance (FHWA 2009, GEC 11, Berg et al. 2009). The present analysis compares the model tests data for top few reinforcements where the normal stresses are low. For lower normal stresses, experimental results suggest a higher value of frictional factor usually greater than one (Koerner 2012, Bergado et al. 2001). Hence a factor equal to one will anyway give a conservative estimation of the pullout capacity.

Table 2 Parameters used for case study

G^*	μ	ϕ_r	α	P_H^*
21.8	9469.5	44	67	1.22
6.8	4132.3	44	67	1.70
3.6	3611.1	44	67	1.99
2.3	4034.3	44	67	2.12
1.6	5778.4	44	67	2.17
1.2	15530.1	44	67	2.07

Note: G=38462 kPa, k_s=40793 kN/m3 (Bathurst et al. 2009; Patra and Shahu 2012), shear layer thickness H=3.5 mm as obtained from Alshibli and Sture (1999)

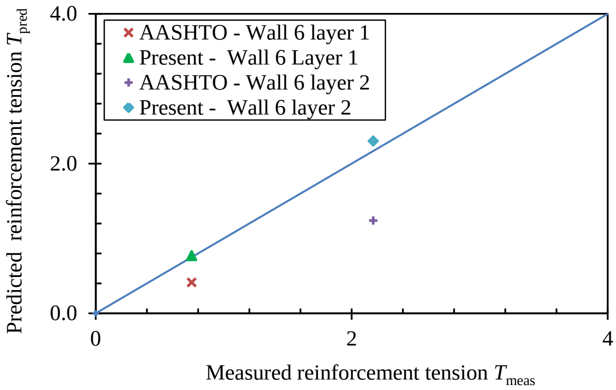

Figure 18 Measured (Bathurst et al. 2009) versus predicted maximum reinforcement tension

6. CONCLUSION

In this paper, a novel approach is proposed for the analysis of an inextensible reinforcement resting on a linear elastic Pasternak subgrade and subjected to an oblique pullout force. The result of the analysis can be directly incorporated for the internal stability analysis of reinforced soil walls.

An updated discretization technique is used to determine the exact deformed shaped of reinforcement. The present analysis demonstrates that under the transverse displacement the reinforcement experiences a higher value of rigid displacement u_A along the horizontal direction. Higher the rigid displacement u_A, lower is the mobilized tension in the reinforcement. The decrease in reinforcement tension is more for lower values of G^* and μ, and higher values of α and ϕ_r. However, the tension in the reinforcement becomes more localized at the pullout end for higher values of the rigid displacement.

As subgrade shear stiffness factor G^* increases, the horizontal component of projected length increases and becomes equal to the initial length of the reinforcement. The above increase is found to be greater for lower values of G^* but higher values of normal stiffness factor μ, angle of interface friction ϕ_r and obliquity α of the pullout force. In few cases, the horizontal projected length may become as low as eighty per cent of the initial length of the reinforcement.

All the responses namely, end displacement, mobilized maximum reinforcement tension and pullout capacity show a significant difference after length correction compared to no correction. The effect of length correction is predominant for lower values of G^*.

As the obliquity α of the pullout capacity increases, the uncorrected values of horizontal component of the pullout capacity P_H^* goes on increasing. However, for a greater angle of obliquity α (> 60), the corrected pullout capacity again reduces which is also evident as reported by Shahu (2007).

Because, the normal and shear stresses at the soil-reinforcement interface increase with the increase in obliquity α of the pullout force thereby the pullout capacity P_H^* increases. At the same time, with the increase in obliquity α there is an increase in the rigid body displacement u_A or, decrease in the projected length of the reinforcement. As the projected length reduces, there is a reduction in the mobilized reinforcement tension and horizontal component of oblique pullout capacity P_H^*. For a higher value of the obliquity α, the above reduction in the pullout capacity arisen from the lesser projected length may dominate over the increase in the pullout capacity due to the greater interface shear stresses.

A length correction factor is introduced in the analysis and its effect on the pullout capacity is studied. The analysis shows a significant effect of the length correction on the pullout responses: pullout capacity, mobilized reinforcement tension and end displacement. There is a 15-20 % decrease in all the responses particularly for high values of obliquity and interface frictional angle and lower values of normal and subgrade shear stiffness factor. A case study is also presented and the maximum reinforcement tension is predicted for top few reinforcements using the proposed method and the AASHTO Simplified Method. The present analysis gives a better prediction of the mobilized reinforcement tension compared to the AASHTO method. Thus, the present analysis gives a better prediction of the pullout capacity, mobilized reinforcement tension and end displacement which is useful for a more rational design of reinforced earth retaining structures.

List of Symbols

α	obliquity of the end-force
D	overburden depth (m)
Δx	length of reinforcement element along x-axis (m)
Δs	length of reinforcement element after deformation (m)
E_s	modulus of elasticity (kN/m^2)
G	shear modulus (kN/m^2)
γ	unit weight of the soil (kN/m^3)
G^*	subgrade shear stiffness factor= $GH/\gamma DL$
H	shear layer thickness (m)
k_s	modulus of subgrade reaction or spring constant (kN/m^3)
L	total length of reinforcement (m)
L_H	projected horizontal length (m)
μ	subgrade normal stiffness factor = $K_s L/\gamma D$
n	total number of elements
ν	poisson's ratio
p, q	vertical stresses at the top and the bottom surfaces of reinforcement (kN/m^2)
P	oblique end-force (kN/m)
ϕ	angle of shearing resistance of soil
ϕ_r	angle of interface shearing resistance between soil and reinforcement
P^*	normalized oblique pullout force = P/T_{HP}
P_H^*	normalized horizontal component of oblique pullout force
S_v	vertical spacing of reinforcement (m)
f_1, f_2	friction stresses or soil-reinforcement interface shear resistance on the top and bottom surface of the reinforcement (kN/m^2)
T,$T+\Delta T$	tension in the reinforcement at distance x and $x+\Delta x$ respectively (kN/m)
T_{HP}	axial pullout capacity = 2 $\gamma DL\tan\phi_r$ (kN/m)
$T_{\max}^*$	normalized maximum tension in reinforcement

$\theta, \theta+\Delta\theta$ slope of reinforcement with horizontal at distance x and $x+\Delta x$
T^* normalized tension = T/T_{HP}
w vertical displacement of the reinforcement (m)
W normalized displacement = w/w_L
x, z horizontal and vertical axes
X normalized distance = x/L

Subscripts

c centre
H horizontal component
i node or element or iteration
L value at X = 1
max maximum
0 value at X = 0

7. REFERENCES

AASHTO (2002). Standard Specifications for Highway Bridges, 17th edn, American Association of State Highway and Transportation Officials (AASHTO), Washington, DC.

Allen, T. M. and Bathurst, R. J. (2013). “Design and Performance of 6.3-m-High, Block-Faced Geogrid Wall Designed Using K-Stiffness Method.” Journal of Geotechnical and Geoenvironmental Engineering, 140, Issues 2, pp 04013016-1-12.

Alshibli, K. A., and Sture, S. (1999). “Sand shear band thickness measurements by digital imaging techniques.” Journal of computing in civil engineering, American Society of Civil Engineers, 13, Issues 2, pp103–109.

Bathurst, R.J., Walters, D.L., Hatami, K. and Allen, T.M. (2001) “Full-scale Performance testing and numerical modelling of reinforced soil retaining walls.” Landmarks in Earth Reinforcement: Proceedings of the International Symposium on Earth Reinforcement, Fukuoka, Kyushu, Japan, 14-16 November, 2001. Taylor & Francis, US.

Bathurst, R., Nernheim, A., Walters, D., Allen, T., Burgess, P., and Saunders, D. (2009). “Influence of reinforcement stiffness and compaction on the performance of four geosynthetic-reinforced soil walls.” Geosynthetics International, Thomas Telford Ltd, 16, Issues 1, pp43–59.

Berg, R. R., Christopher, B. R., and Samtani, N. C. (2009). “Design of mechanically stabilized earth walls and reinforced soil slopes.” FHWA GEC 011, Vol. I, National Highway Institute, Federal Highway Administration, U.S. DOT, Washington, DC.

Bergado, D., Voottipruex, P., Srikongsri, A., and Teerawattanasuk, C. (2001). “Analytical model of interaction between hexagonal wire mesh and silty sand backfill.” Canadian Geotechnical Journal, NRC Research Press, 38, Issues 4, pp782–795.

Damians, I.P., Bathurst, R. J., Adroguer, E. G., Josa, A. and Lloret, A. (2016). “Environmental assessment of earth retaining wall structures.” Environmental Geotechnics, Thomas Telford Ltd. http://dx.doi.org/10.1680/jenge.15.00040.

Gao, Y., Yang, S., Wu, Y., Li, D. and Zhang, F. (2014). “Evaluation of oblique pullout resistance of reinforcements in soil wall subjected to seismic loads.” Geotextiles and Geomembranes, 42, pp515–524.

Koerner, R. M. (2012). “Designing With geosynthetics.” 6th Ed., Prentice- Hall, Englewood Cliffs, N.J.

MacLaughlin, M., Sitar, N., Doolin, D., and Abbot, T. (2001). “Investigation of slope-stability kinematics using discontinuous deformation analysis.” International Journal of Rock Mechanics and Mining Sciences, 38, pp753–762.

Madhav, M. R., and Umashankar, B. (2003). “Analysis of inextensible sheet reinforcement subject to transverse displacement/force: Linear subgrade response.” Geotext. Geomembr., 21, Issues 2, pp69-84.

Ouria, A., Toufigh, V., Desai, C., Toufigh, V. and Saadatmanesh, H. (2016). “Finite element analysis of a CFRP reinforced retaining wall.” Geomechanics and Engineering, 10, Issues 6, pp757-774.

Patra, S., and Shahu, J.T. (2012). “Pasternak model for oblique pullout of inextensible reinforcement”, J. Geotech. Geoenviron. Eng., 138, Issues 12, pp1503-1513.

Rowe, R. K. & Ho, S. K. (1993). Keynote lecture: A review of the behaviour of reinforced soil walls. Proceedings of the international symposium on earth reinforcement practice (eds H. Ochiai, S. Hayashi and J. Otani), vol. 2, pp. 801–830. Rotterdam, the Netherlands: Balkema.

Selvadurai, A. P. S. (1979). “Elastic analysis of soil-foundation interaction.” Developments in geotechnical engineering, Vol. 17, Elsevier, Amsterdam, Netherlands.

Shahu, J. T. (2007). “Pullout response of inextensible sheet reinforcement subject to oblique end-force.” J. Geotech. Geoenviron. Eng., 133, Issues 11, pp1440–48.

Sitar, N., MacLaughlin, M.M. and Doolin, D.M. (2005). “Influence of kinematics on landslide mobility and failure mode.’” Journal of geotechnical and geoenvironmental engineering, 131, pp 716–728.

Vlazov, V. Z., and Leontiev, U. N. (1966). “Beams, plates and shells on elastic foundations.” Israel Program for Scientific Translations, Jerusalem (translated from Russian).

Wang, H. B., and Anderson, M. P. (1982). “Introduction to ground water modeling: Finite difference and finite element methods.” Academic, London.

Won, M.-S., Lee, O.-H., Kim, Y.-S., Choi, S.-K. (2016). “A 12-year long-term study on the external deformation behavior of Geosynthetic Reinforced Soil (GRS) walls.” Geomechanics and Engineering, 10, Issues 5, pp565-575.

Yu, Y., Bathurst, R. J., and Allen, T. M. (2016). “Numerical Modeling of the SR-18 Geogrid Reinforced Modular Block Retaining Walls.” Journal of Geotechnical and Geoenvironmental Engineering, 142, Issues 5, pp04016003-1-13.